Journal of The Electrochemical Society, **166** (8) D354-D358 (2019)
0013-4651/2019/166(8)/D354/5/$38.00 © The Electrochemical Society

Mechanisms of Localized Pulsed Electrodeposition (L-PED) for Microscale 3D Printing of Nanotwinned Metals

Reza Morsali, Dong Qian, and Majid Minary-Jolandan[*,z]

Department of Mechanical Engineering, The University of Texas at Dallas, Richardson, Texas 75080, USA

Nanotwinned metals (nt-metals) show larger ductility and strength compared to nanocrystalline metals facilitated by their special microstructure containing arrays of parallel twin boundaries. The recently-introduced localized pulsed electrodeposition (L-PED) enables 3D printing of nt-metals in complex geometries. Herein, the first computational model incorporating all the involved physics (i.e. electrodeposition, evaporation, fluid flow, and heat transfer) in the L-PED process is presented. The model reveals the critical rules of the pulsed signal and evaporation-driven convection flux in the mass transport mechanism, ion concentration, current density, and printing rate in the L-PED process. Notably, the simulation results predict a very high peak current density (∼130 times of the average current density) during the short (∼ms) ON-time. This high current density in a short period of ON-time results in high deposition rate, of possibly a metal with high internal stress. This prediction may explain the current hypotheses in the literature on formation of nt-metals by stress relaxation during the OFF-time.

[DOI: 10.1149/2.0051910jes]

Manuscript submitted February 27, 2019; revised manuscript received April 29, 2019. Published May 21, 2019.

Major emphasis in additive manufacturing (AM) of metals is placed on controlling the microstructure of the printed metal, since the microstructure determines mechanical and electrical properties. Recently, the localized pulsed electrodeposition (L-PED) process that enables microscale three-dimensional (3D) printing of a special class of metals, termed nanotwinned metals (nt-metals) was introduced.[1–3] Nt-metals have a unique crystalline microstructure with grains containing a high density of layered nanoscale twins divided by coherent twin boundaries (TBs). TBs effectively block dislocation motion while facilitating ductility, which overall result in higher ductility and strength in nt-metals compared to their nanocrystalline counterparts.[4–6]

The L-PED is an electrochemical-based microscale metal AM process (μ-AM). In this process, electroplating is confined to a small zone at the tip of a nozzle filled with the electrolyte of the metal of interest (Figure 1A).[7,8] An electrolyte meniscus (liquid bridge) functions as a confined electrochemical bath (Figure 1B). When a pulsed electric potential is applied between the anode and the substrate (cathode), the metal ions are deposited at the growth front within the meniscus area on the cathode surface.[7–10]

In the L-PED process, the applied potential/current is interchanged repeatedly between ON and OFF with the time periods of T_{ON} and T_{OFF}, respectively (Figure 1C). Therefore, during a short time interval of ON potential, a very high current density and subsequently high deposition rate is achieved, while in the OFF-time the consumed ions are recovered, and a higher concentration of ions accumulates on the cathode surface for the subsequent ON-time. In pulsed electrodeposition (PED) the ON-time is often on the order of several milliseconds, and the OFF-time is on the order of several seconds. The L-PED process is capable of printing high purity crystalline metallic structures with different geometries such as free-standing wires, micro-pillars (μ-pillars), and layer-by-layer structures, through precise and controlled motion of the relative position of the nozzle and the substrate.[1–3,7–10]

The L-PED is a multiphysics process involving several transport mechanisms including convection (driven by the rapid electrolyte evaporation at the nozzle tip), migration, and diffusion. These transport mechanisms are affected by short duration ON-pulses, and longer duration OFF-pulses. Subsequently, the ion concentration on the cathode and the current density constantly change in each pulse. These parameters ultimately control the printing rate and the microstructure of the printed metal. Although the exact mechanisms of nanotwin formation in PED are still a matter of debate, it is generally hypothesized that high current density during the short ON-time results in deposition of a metal film with a high internal stress, and the subsequent stress relaxation during the OFF-time results in formation of twins.[6,11–13] Although the L-PED process has been experimentally demonstrated,[1–3] due to the lack of modeling, there is a limited understanding of the multiphysics dynamics that occur in the process. Here for the first time, a computational multi-physics finite element (FE) model is developed to shed light on the important parameters in the L-PED process.

Multi-Physics simulation of the L-PED process.—A two-dimensional (2D) model was developed using the commercial COMSOL Multi-physics package. The model consists of copper (Cu^{2+}) and sulfate ions ($SO_4{}^{2-}$) in an aqueous electrolyte, the surrounding environment (air), and the nozzle, Fig. 1D. The metal ions transport toward the substrate by mass transport mechanisms identified by the Nernst-Planck equation:

$$N_i = -D_i \nabla c_i - z_i u_i F c_i \nabla \varphi_l + c_i u \qquad [1]$$

in which N_i is the transport vector; the diffusivity of the ionic species is denoted by D_i; the concentration of ions, electronic charge of the ionic species, and the mobility of the charged species are shown by c_i, z_i, and u_i, respectively. F is the Faraday constant; the electric potential difference in the solution is shown by φ_l; and u is the fluid velocity.

The metal ions transport from the bulk electrolyte toward the meniscus through three mechanisms: diffusion, migration, and convection, which overall control the printing process. These three fluxes are identified by the first, second, and third terms in Eq. 1, respectively. The migration is only active during t_{on}, while the convection and diffusion are always active. The direction and magnitude of these transport mechanisms in the L-PED process are time-dependent, in contrast to the direct current electrodeposition (DC-ED).[9,10] The boundary condition for the cathode surface is charge-transfer reaction kinetics defined by the Butler-Volmer expression:

$$i_{ct} = i_0 \left\{ C_R \exp\left(\frac{\alpha_a F \eta}{RT}\right) - C_0 \exp\left(\frac{-\alpha_c F \eta}{RT}\right) \right\} \qquad [2]$$

where i_{ct} is the local current density, i_0 is exchange current density, α_a and α_c are charge transfer coefficients for the anode and cathode electrodes, respectively, η is the overpotential, $C_{cu^{2+}}$ and $C_{cu^{2+},ref}$ are the concentration of Cu^{2+} ions on the electrode surface and within the bulk electrolyte, respectively. The printing rate, v_p, is directly proportional to i_{ct}, and can be expressed as:

$$v_{dep} = -\frac{M_{Cu}\, i_{ct}}{z_{cu}\, r_{Cu}\, F} \qquad [3]$$

in which M_{Cu} is the molar mass and ρ_{Cu} is the density of copper.[14] Parameters in above equations were obtained from the literature.[15–21]

Water evaporation from the meniscus surface has a significant effect on the process. Heat and mass transfer formulation was taken into account to model the evaporation. The governing equation for heat

---

[*] Electrochemical Society Member.
[z] E-mail: majid.minary@utdallas.edu

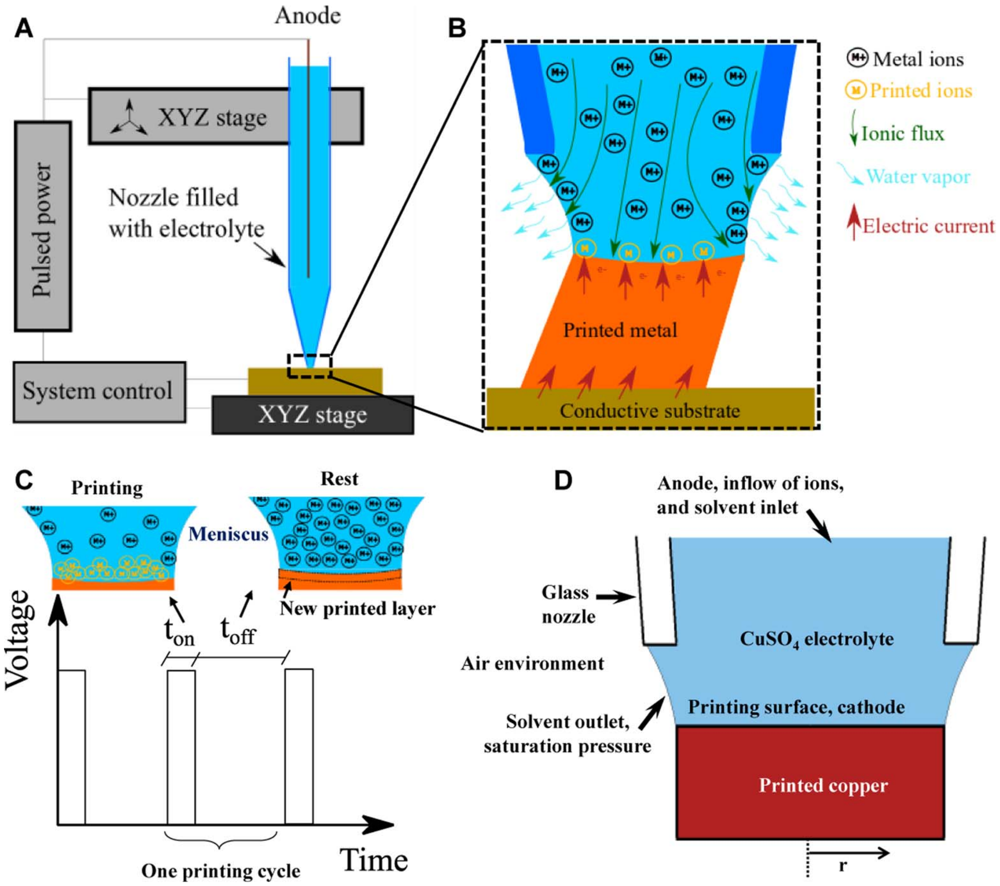

Figure 1. (A) The schematic of the microscale 3D metal printer based on the localized pulsed electrodeposition (L-PED). (B) The close-up view of the liquid bridge (meniscus) at the nozzle tip. (C) A pulsed (electrodeposition) cycle including t_{on} and t_{off}. Metal is printed during the t_{on} while during the t_{off} no deposition occurs. (D) The constituents and boundary conditions of the multiphysics model.

transfer for the all the domains is:

$$\rho C \left(\frac{\partial T}{\partial t} + v \bullet \nabla T \right) - K \nabla^2 T = Q \qquad [4]$$

In Eq. 4, C is the heat capacity; T is the temperature; K is isotropic thermal conductivity; Q is the heat source, and v is the velocity. The Neumann type boundary condition was applied for heat transfer on the free surface of the meniscus.[22] Evaporation process was modeled by using diffusion equation within the air environment:[23]

$$\frac{\partial c_v}{\partial t} = D_v \nabla^2 c_v \qquad [5]$$

where c_v denotes vapor concentration, and D_v is diffusivity of water vapor in air. Given by the ideal gas law, the saturated vapor concentration is applied to the meniscus surface (Fig. 1D). Water evaporation generates convective flow within the electrolyte domain. The Navier-Stokes and continuity equations were solved together to determine the fluid flow. The equation for the shape of the meniscus has been previously reported in Refs. 7,24.

The diffusivity of the Cu^{2+} ions was considered to be 5×10^{-7} cm^2/s. The values for the constants were: $i_0 = 0.003$ A/cm^2; the sum of the charge transfer coefficients for the anode and cathode electrodes is equal two ($\alpha_a + \alpha_c = 2$) since the discharge of Cu^{2+} ions is a two-electron transfer process per ion. The values of transfer coefficients have been calculated experimentally to be $\alpha_a = 0.5$ and $\alpha_c = 1.5$;[25,26] $C_0 = \frac{C_{cu^{2+}}}{C_{cu^{2+},ref}}$; $C_R = 1$; where $C_{cu^{2+}}$ and $C_{cu^{2+},ref}$ are the concentration of Cu^{2+} ions on the electrode surface and in the bulk electrolyte, respectively. The viscosity and density of the solution were assumed to be 0.0010093 Pa.s and 1000 kg/m^3, respectively. The concentration of the ions in the bulk electrolyte and the diameter of the deposited metal wire (D) were set to 100 mM and 0.7 µm, respectively, based on experimental data.[2] The relative humidity of the environment (RH) was set at 70% throughout the process.

In the simulation, a pulsed voltage of 0.4 V was applied between the anode and cathode, with t_{on}: t_{off} of 20 ms: 2 s as shown in Fig. 2A. Figure 2B shows the resulting current density and the printing rate (the rate of deposition) during one cycle. According to Eq. 2 and Eq. 3, the deposition rate and current density have the same trend. The results show that the current density rapidly increases from zero to a large peak value over ~2 A/cm^2, within ~ 2 ms. Correspondingly, the deposition rate rapidly increases to more than ~ 751 nm/s. Afterwards, the current density and deposition rate slowly decreases to final values of ~ 0.92 A/cm^2 and 340 nm/s, respectively, just before the electric pulse is turned off. At this point, metal deposition is interrupted and no deposition occurs during t_{off}.

In the process, the nozzle continuously moves with a fixed speed (during the on-off cycle), and the ion transport mechanisms collectively accommodate the high deposition rate in a short ON-time. The average values of the deposition rate and current density are obtained by integrating over the entire on-off cycle. Table I presents the details values for the peak and average current density and printing rate. The simulation predicts an average current density (I_{avg}) of ~ 0.0157 A/cm^2 over one cycle ($T_{ON} + T_{OFF}$), while the average current density over the ON-time is ~ 1.15 A/cm^2. The ratio of the peak current density to average current density (I_p / I_{avg}) is ~130. Correspondingly, the ratio of the peak deposition rate to average deposition rate is ~130. The peak deposition rate is ~750 nm/s, while the average deposition rate during the ON-time and the average deposition rate during the entire cycle are ~ 421 nm/s and 5.8 nm/s. The overall average deposition rate of the process for an average current

Table I. Results of the computational model for the current density and deposition rate in the L-PED process.

Peak current density (I_p) [A/cm^2]	Average current density over t_{on} [A/cm^2]	Average current density over one cycle (I_{avg}) [A/cm^2]	Current density ratio (I_p/I_{avg})
2.04	1.15	0.0157	130
Peak deposition rate (v_p)[nm/s]	Average deposition rate over t_{on}[nm/s]	Average deposition rate over one cycle (V_{avg})[nm/s]	Deposition rate ratio (v_p/v_{avg})
751	421	5.78	130

density of 157 mA/cm^2 is ∼ 5.8 nm, which matches very well with the experiment.[3]

As the simulation results predict, a very high peak current density (∼130 times of the average current density) occurs in the L-PED process. This high current density, results in high average deposition rate (∼420 nm/s) in a short time (∼20 ms). It can be expected that such high deposition rate would result in formation of a metal film with a high internal stress. It is generally argued that stress relaxation during the t_{off} results in formation of twins.[6,11–13] This is supported by the direct in situ experimental investigation of stress evolution via precise measurement of a flexible cathode deflection during deposition process.[12] In this experiment, a periodic increase in tensile stress and stress relaxation was observed during the ON time and OFF time, respectively.[12] In addition, molecular dynamic simulations has shown that due to the high level of stress during the ON-time the twin nuclei originate at the triple junctions of GBs (grain boundaries), and during the OFF-time they are extended along the lateral (111) direction. The consecutive nucleation and extension results in growth of nt-Cu microstructure.[13]

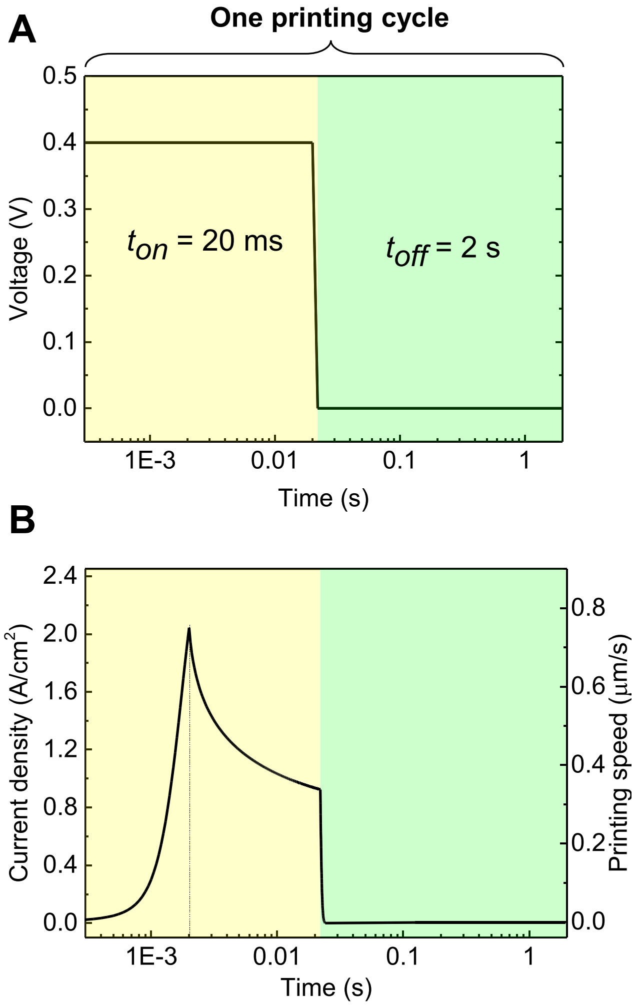

Figure 2. (A) The applied pulsed voltage vs. time over one printing cycle (ON/OFF) in the L-PED process. t_{on} is only 1% of the process duration, so a logarithmic scale was used to expand the time axis over t_{on}. The yellow and green regions in the graphs represent t_{on} and t_{off}, respectively. (B) The current density, and the average printing rate (v_p) over the cathode surface vs. time.

The ion concentration close to the cathode surface control the deposition rate. The metal ion concentration and flux map of ions at the end of t_{off} and t_{on} are shown in Fig. 3. The total flux is the summation of the diffusion, convection and migration fluxes (Fig. 3E). The simulation results show that the average concentration of ions in the meniscus at the end of t_{off} is ∼2.4 times larger than the bulk electrolyte (∼240 mM), Fig. 4A. This high concentration at the end of t_{off} facilitate the high deposition rate during the ON-time in the subsequent cycle (Fig. 3A). During the ON-time metal ions are rapidly consumed, which brings down the ionic concentration to ∼16 mM at the end of the ON-time, which is more than 6-times lower than the bulk electrolyte. In Fig. 4A, the average concentration of ions in the meniscus is also shown for the DC-ED (direct current electrodeposition) for comparison, which is constant throughout the process at ∼16 mM.

Figure 3B shows the convection flux within the meniscus at the end of the ON-time and OFF-time. The source of this convection flux is the evaporation of the electrolyte at the meniscus free surface, which generates a convective flow within the nozzle. Such convective flux is not present in the conventional bulk electrodeposition. It turns out that the evaporation has a significant role in the L-PED process. The evaporation and the resulting convection flux increases the printing rate. It also eliminates the need for having an external pump in the system, since evaporation-driven convention flux functions as a natural pump. This forced convection steadily pumps the ions from the bulk electrolyte into the meniscus and increases the ion concentration, in particular during the t_{off} (Fig. 4B).

Evaporation at sub-micron is fast enough to drain equivalent to several thousand meniscus volumes every second.[9,10] To highlight the role of evaporation, the magnitude of the fluxes entering the meniscus, for the case without any evaporation in the system, was also calculated from the simulations (Fig. 4C). In the presence of evaporation, the convection generates a positive total flux during the t_{off} and eventually the ion concentration on the cathode increases to ∼2.4 times larger than the bulk solution (Fig. 3A). Without evaporation, however, the concentration of ions never increases above the concentration of the bulk electrolyte. In addition, when evaporation is not present, the magnitude of the total flux significantly reduces (Figures 4B and 4C). Figures 4B and 4C show the amount of ions pass into the meniscus per second (mol/s). The maximum flux reduces from over 100 femtomol/s to ∼40 femtomol/s.

The forced convection steadily pumps the ions from the bulk electrolyte into the meniscus and increases the ion concentration, in particular during t_{off}. On the other hand, the high concentration gradient prompts the back-diffusion from the meniscus toward the bulk electrolyte (Fig. 3C). The direction of convection flux is always from the bulk electrolyte toward the meniscus surface where evaporation happens. The direction of diffusion changes over time based on the concentration gradient. It is toward the printing surface at the end of t_{on}, and toward the bulk electrolyte at the end of t_{off}, since the concentration of ions increases while no deposition occurs during the OFF-time. When the t_{on} starts, metallic ions get consumed on the printing surface. The low concentration of ions within the meniscus reverses the

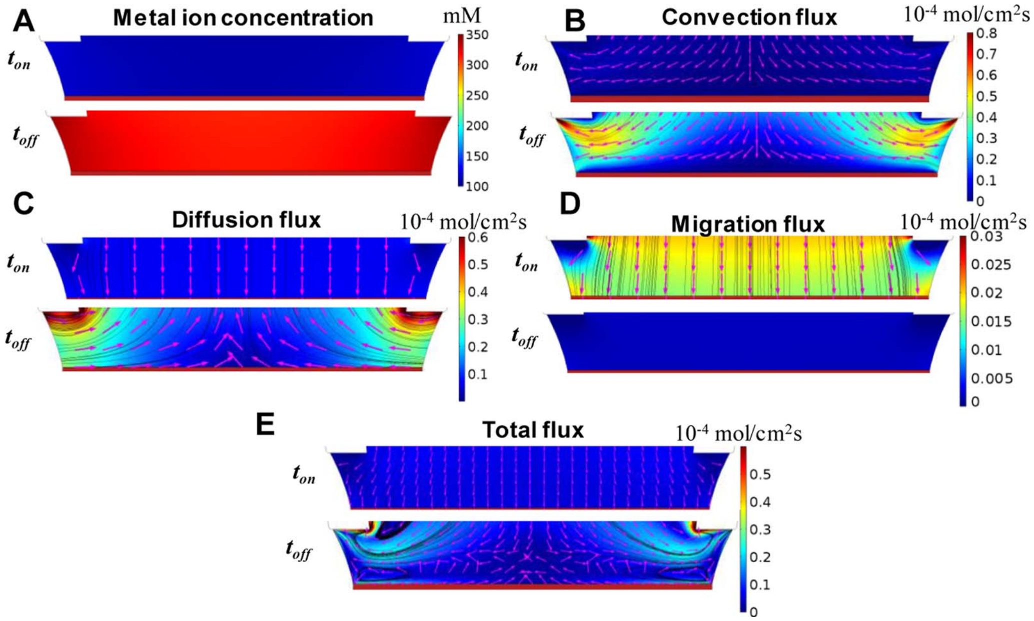

Figure 3. The distribution of the (A) concentration of metal ions, (B) convection flux, (C) diffusion flux, (D) migration flux, and (E) total flux within the meniscus at the end of t_{on} and t_{off}.

diffusion direction. Although the magnitude of the flow velocity (u in Eq. 1) is constant over time because of the time-independent evaporation, variation of the concentration (c in Eq. 1) changes the magnitude of the convection flux over time. Interestingly, the convective flux is more intense at the top and bottom corners of the meniscus where the evaporation is higher.

The migration is the third transport mechanism. This mechanism is only active during the t_{on} and is toward the printing surface, since

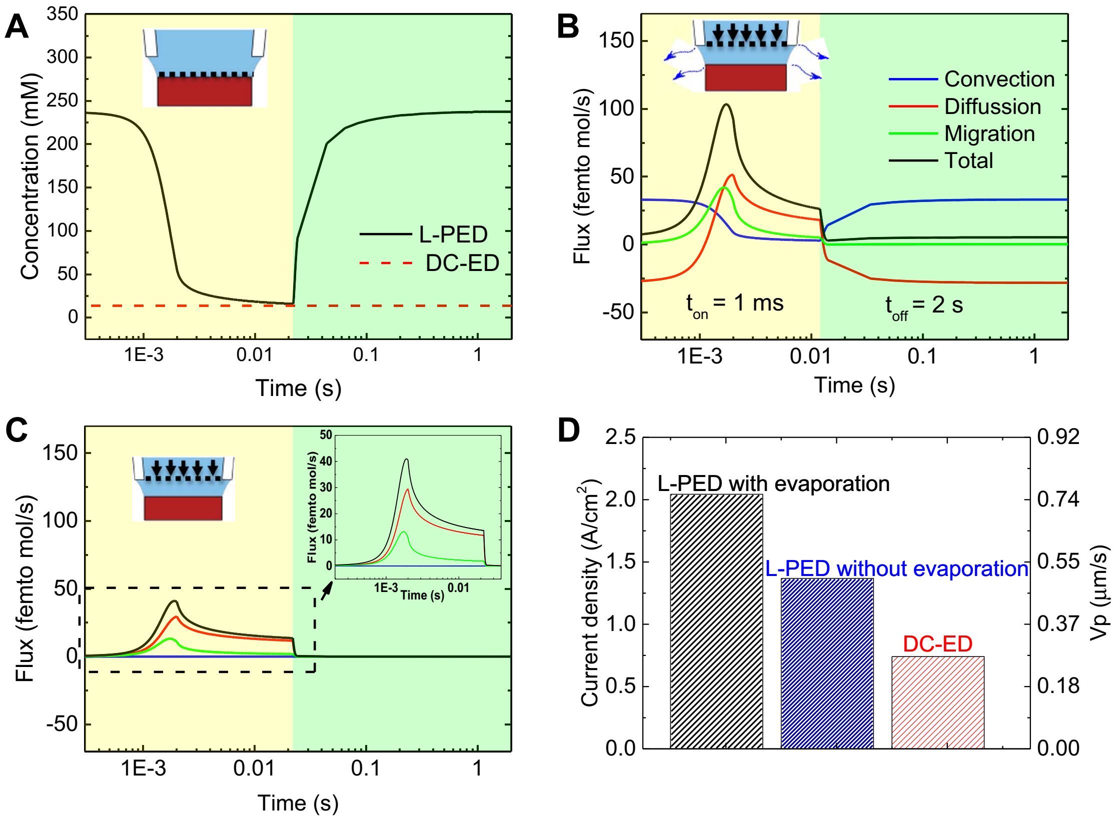

Figure 4. (A) The average concentration of metal ions on the printing surface for L-PED and DC-ED vs. time. The predicted values for fluxes vs. time for (B) the case with evaporation and (C) the case without evaporation. (D) The comparison of the peak current density, and peak deposition rate in L-PED with and without evaporation, and DC electrodeposition.

no voltage is applied during the OFF-time. The total flux is the contribution of three fluxes (Fig. 3E). With the three fluxes downward during the t_{on}, the total flux is toward the cathode surface, which compensates for the deposited ions on the cathode. It can be observed that the migration flux has a relatively smaller contribution to the total flux (Fig. 3D and Fig. 4B). Flux vortices observed in the two sides of the meniscus at the end of t_{off} is due to the opposite direction of convention flux and diffusion flux (Figure 3E).

It is known that the average current density in PED is lower than the current density in DC-ED.[3] As shown in Fig. 4A, the average ion concentration vs. time in the DC-ED is constant and much lower than that of the L-PED. Similarly, the peak current density in the L-PED is much larger than the DC case. Consequently, the peak deposition rate in the PED is much larger (~172%) than the DC-ED, Fig. 4D. (The predicted v_p in DC-ED is 272 nm/s, which is fairly close to the experimental value of ~250 nm/s.[2]) In the same plot (Fig. 4D) these parameters are also shown for the case of L-PED without evaporation. The higher concentration caused by evaporation results in ~49% larger maximum v_p in for the case with evaporation compared to the case without evaporation. The very high peak current density in each cycle of PED results in formation of high nucleation sites during the ON-time and formation of the high stress metal deposit. The stress relaxation during the t_{off} results in formation of twins.[27,28]

In conclusion, the presented multi-physics simulation, for the first time, provides insight into the dynamics of L-PED process for 3D printing of nanotwinned metals. An important distinction between the PED and DC-ED is the formation of nanotwinned microstructure in the former vs. nano- or micro-crystalline microstructure in the latter. The simulation results can explain this difference on the basis of ionic concentration on the cathode surface, current density, and the deposition rate. The simulation results predict a very high peak current density (~130 times of the average current density) occurs in the L-PED process. This high current density, results in high average deposition rate (~420 nm/s) in a short time (~20 ms). It can be expected that such high deposition rate would result in formation of a metal film with a high internal stress. The subsequent stress relaxation during the t_{off} results in formation of twins. During the short (~ms) ON-time, the ion concentration gradually decreases due to the ion consumption by metal deposition. The combination of evaporation and OFF-time provide a unique condition for concentration to increase in L-PED. The OFF-time enables recovering the consumed ions during deposition, and provides higher concentration of ions on the cathode for the subsequent ON-time. The simulation here, only considers the dynamics of the electrolyte, ion concentration, and current density. Detailed atomistic simulations are required to investigate changes in the microstructure of the deposited metal during OFF-time.

Acknowledgments

This work was supported by the NSF-CMMI (award # 1727539), the US Office of Naval Research (award # N00014-15-1-2795), and NASA-SBIR award No. 80NSSC18P2193 subcontract from NANORANCH company.

ORCID

Reza Morsali https://orcid.org/0000-0002-5063-1631

References

1. A. Behroozfar, S. Daryadel, S. R. Morsali, S. Moreno, M. Baniasadi, R. A. Bernal, and M. Minary-Jolandan, *Adv. Mat.*, **30**, (2018).
2. S. Daryadel, A. Behroozfar, S. R. Morsali, S. Moreno, M. Baniasadi, J. Bykova, R. A. Bernal, and M. Minary-Jolandan, *Nano Lett.*, **18**, 208 (2018).
3. S. Daryadel, A. Behroozfar, and M. Minary-Jolandan, *Adv. Eng. Mat.*, **21**, 1800946 (2019).
4. L. Lu, X. Chen, X. Huang, and K. Lu, *Science*, **323**, 607 (2009).
5. K. Lu, L. Lu, and S. Suresh, *science*, **324**, 349 (2009).
6. K. Lu, *Nat. Rev. Mater.*, **1**, 16019 (2016).
7. J. Hu and M.-F. Yu, *Science*, **329**, 313 (2010).
8. A. P. Suryavanshi and M.-F. Yu, *Appl. Phy. Lett.*, **88**, 083103 (2006).
9. S. Morsali, S. Daryadel, Z. Zhou, A. Behroozfar, M. Baniasadi, S. Moreno, D. Qian, and M. Minary-Jolandan, *J. of Appl. Phy.*, **121**, 214305 (2017).
10. S. Morsali, S. Daryadel, Z. Zhou, A. Behroozfar, D. Qian, and M. Minary-Jolandan, *J. of Appl. Phy.*, **121**, 024903 (2017).
11. D. Xu, W. L. Kwan, K. Chen, X. Zhang, V. Ozoliņš, and K. N. Tu, *Appl. Phy. Lett.*, **91**, 254105 (2007).
12. D. Xu, V. Sriram, V. Ozolins, J.-M. Yang, K. N. Tu, G. R. Stafford, and C. Beauchamp, *J. of Appl. Phy*, **105**, 023521 (2009).
13. G. Cheng, H. Li, G. Xu, W. Gai, and L. Luo, *Sci. rep.*, **7**, 12393 (2017).
14. C. Multiphysics, 5.4, User's Manual, Comsol Inc, in.
15. J. T. Hinatsu and F. R. Foulkes, *J. of The Electrochem. Soc.*, **136**, 125 (1989).
16. T. Hayashi, S. Matsuura, K. Kondo, K. Kataoka, K. Nishimura, M. Yokoi, T. Saito, and N. Okamoto, *J. of The Electrochem. Soc.*, **162**, D199 (2015).
17. T. Braun and D. Schwartz, *J. of The Electrochem. Soc.*, **162**, D180 (2015).
18. D. R. Turner and G. R. Johnson, *J. of The Electrochem. Soc.*, **109**, 798 (1962).
19. E. Mattsson and J. O. M. Bockris, *Trans. of the Faraday Soc.*, **55**, 1586 (1959).
20. W. Zeng, M. L. Free, and S. Wang, *ECS Trans.*, **72**, 23 (2016).
21. V.-H. Hoang and K. Kondo, *J. of The Electrochem. Soc.*, **164**, D564 (2017).
22. B. Rajneesh, F. Xiaohua, and A. Daniel, *New J. of Phy.*, **11**, 075020 (2009).
23. R. Mollaret, K. Sefiane, J. R. E. Christy, and D. Veyret, *Chem. Eng. Res. and Design*, **82**, 471 (2004).
24. V. A. Tatarchenko, *J. of Crys. Growth*, **37**, 272 (1977).
25. E. Mattsson and J. M. Bockris, *Trans. of the Faraday Soc.*, **55**, 1586 (1959).
26. D. Turner and G. Johnson, *J. of The Electrochem. Soc.*, **109**, 798 (1962).
27. I. Utke, P. Hoffmann, and J. Melngailis, *J of Vacu. Sci. & Techn. B: Microelectronics and Nanometer Structures Processing, Measurement, and Phenomena*, **26**, 1197 (2008).
28. J. A. Lewis, *Adv. Func. Mat.*, **16**, 2193 (2006).